Chemically Ordered Pt-Co-Cu/C as Excellent Electrochemical Catalyst for Oxygen Reduction Reaction

Libo Zhang[1], Xiangdong Ji[1], Xiaoran Wang[1], Yongqing Fu[2], Hong Zhu[1,*], Terence Xiaoteng Liu[2,*]

[1]State Key Laboratory of Chemical Resource Engineering, Institute of Modern Catalysis, Department of Organic Chemistry, Beijing Engineering Centre for Hierarchical Catalysts, School of Science, Beijing University of Chemical Technology, Chaoyang, Beijing, 100029, China

[2]Faculty of Engineering and Environment, Northumbria University, Newcastle upon Tyne, NE1 8ST, UK

Corresponding author:

Dr Terence X. Liu, E-mail: terence.liu@northumbria.ac.uk

Prof. Hong Zhu, E-mail: zhuho128@126.com

Abstract

This paper reveals the ordered structure and composition effect to electrochemical catalytic activity towards oxygen reduction reaction (ORR) of ternary metallic Pt-Co-Cu/C catalysts. Bimetallic Pt-Co alloy nanoparticles (NPs) represent an emerging class of electrocatalysts for ORR, but practical applications, e.g. in fuel cells, have been hindered by low catalytic performances owning to crystal phase and atomic composition. Cu is introduced into Pt-Co/C lattices to form $PtCo_xCu_{1-x}/C$ (x=0.25, 0.5 and 0.75) ternary-face-centered tetragonal (fct) ordered ternary metallic NPs. The chemically ordered Pt-Co-Cu/C catalysts exhibit excellent performance of 1.31 A mg^{-1}_{Pt} in mass activity and 0.59 A cm^{-2}_{Pt} in specific activity which are significantly higher than Pt-Co/C and commercial Johnson Matthey (JM) Pt/C catalysts, because of the ordered crystal phase and composition control modified the Pt-Pt atoms distance and the surface electronic properties. The presence of Cu improves the surface electronic structure, as well as enhances the stability of catalysts.

Keywords： Proton exchange membrane fuel cell; oxygen reduction reaction; chemically ordered structure; ternary; mass activity;

Introduction

Proton exchange membrane fuel cells (PEMFCs) have gained growing attention owning to high-energy conversion efficiency, high power density, and low environmental impact. Active carbon support Pt catalysts has been recognized as the most effective catalyst for oxygen reduction and hydrogen oxidation reactions. [1–5] However, the high cost of noble metal resources and insufficient electrocatalytic performances for the oxygen reduction reaction (ORR) on cathode side hinders its large-scale commercialization. It has been proven that Pt alloying transition metal M (M= Ni, Fe, Co, Cu and Zn) could enhance the ORR activity, as well as reduce the Pt loading for cost effective purposes. [6–8] Within the catalysts, the crystal phase of Pt alloys nanoparticles (NPs) is better of chemically ordered structure to prevent structural damage during ORR while operating the PEMFC under harsh environment because it has been found that atomically disordered catalysts structure will lead to a drastic decreased on catalytic activity, thereby the fuel cell performance.[9–11] Chemically ordered structure Pt based alloy catalysts showed high degree of alloying and homogenous atomic distribution.[12] In order to convert the disordered structure to chemically ordered structure NPs, additional treatments are needed, e.g. Cai *et al.* reported that the catalysts annealed at high-temperature showed superior catalytic performance than commercially available Johnson Matthey (JM) Pt/C.[13] High-temperature annealing has been used to increase the catalysts' alloying degree and regulate the crystal phase structure of the catalysts.[14] The chemically ordered structure PtM alloy catalysts have been used effectively to hinder the dissolution of

the transition metals M to improve the Pt based catalysts stability. The chemically ordered structure catalysts present distinctive features of uniform atomic distribution and high alloying degree, and their atoms are arranged in an ordered form compared to that of the disordered PtM alloy catalysts. [15–19]

Up to now, ordered bimetallic catalysts have been proved to have superior activity and stability towards ORR. e.g. PtCo, PtFe, PtCu, and PtCr.[20–28] Recently, ternary nanoparticles have gained growing attention as promising catalysts to enhance catalytic performances by providing more possibilities to modify the crystal phase of existing PtM catalysts.[29–33] Introducing third metal elements to the present binary catalysts for catalytic materials has been used to achieve superior catalytic performances. The improved catalytic performances are attributed to the optimizations of physiochemical structures of Pt such as the modification in the Pt 5d band vacancy, the number of Pt nearest neighbors, Pt and Pt atoms distance, and the surface electronic properties.[12] In particular, ternary alloyed Pt–Co–Cu/C nanoparticles demonstrate excellent catalytic performances as both Pt–Cu or Pt–Co catalysts have been reported better performances for the ORR.[34–37] Here we prepared a series of $PtCo_xCu_{1-x}$/C catalysts which have shown further improved ORR activity and better stability compare to above mentioned bimetallic NPs. Briefly, Carbon supported chemically ordered structure PtCo/C was firstly synthesized by an impregnation method, followed by annealing at 700 ^oC for 2 hours in 5% H_2 environment. Then, various ratios of Cu atoms merely served as the substitute for Co to the lattice of Pt–Co–Cu/C intermetallic possessing the same atomic stack as PtCo/C

intermetallic at the same temperature. The annealing temperature was 700 ºC for ordered structure nanoparticles, the average particle size is 5.0 nm and a homogeneous particle size distribution was obtained. The obtained ordered structure Pt–Co–Cu/C catalysts demonstrated superior catalytic ORR performances when compared to PtCo/C and JM Pt/C catalysts.

Experimental

Materials

Copper nitrate trihydrate ($Cu(NO_3)_2\ 2H_2O$), Cobalt chloride hexahydrate ($CoCl_2\ 6H_2O$), Hexachloroplatinic acid ($H_2PtCl_6\ 6H_2O$), and other reagents were supplied by the Beijing Chemical Factory of China in analytical grade. Nafion solution (5 wt%) was purchased from Dupont. Carbon powder (EC-300J) was obtained from Shanghai Kajet Chemical Reagent Center and was pretreated by hydrogen peroxide to take out surface impurities and to form oxygenous groups. Commercial platinum catalysts (40 wt%, HISPEC4000, denoted as JM Pt/C) were purchased from Johnson Matthey.

Preparation of carbon supported chemically ordered PtCo/C

Ordered PtCo/C with 20 wt% metal loading was prepared by an improved impregnation method. In a synthesis process of ordered PtCo/C alloy NPs with an adding Co to Pt atomic ratio of 1:1, 18.67 mg of $CoCl_2\ 6H_2O$ and 40.7 mg of $H_2PtCl_6\ 6H_2O$, and 80 mg of the EC-300J carbon support was dispersed to 10 ml of deionized water then mixed in ultrasonic sound bath for 30 min to obtain a smooth thick slurry. After drying at 80 ºC in an oven for one night, the black mixture was ground in an

agate mortar. The black powder was annealed in a tube furnace at 200 °C under 95% Ar /5% H_2 flow for 3 h. Then, the sample was annealed at 700 °C under 95% Ar /5% H_2 flowing for 2 h to form chemically ordered structure.

Preparation of carbon supported chemically ordered $PtCo_xCu_{1-x}$/C catalysts

The synthesis procedure of $PtCo_xCu_{1-x}$/C NPs is shown in Scheme 1. Carbon supported $PtCo_xCu_{1-x}$/C (x=0.25, 0.5, and 0.75) with 20 wt% metal loading was synthesized by an improved impregnation method. The metal contents of the Pt-Co-Cu/C catalysts were prepared by controlling the molar ratios of Co, Cu, and Pt precursors. In a synthesis process of $PtCo_xCu_{1-x}$/C alloy NPs, $CoCl_2$ $6H_2O$, $Cu(NO_3)_2$ $2H_2O$, and H_2PtCl_6 $6H_2O$ precursors with regulating molar ratios were dispersed in deionized water, and then 80 mg of the EC-300J carbon support was dispersed to 10 ml of deionized water then mixed in ultrasonic sound bath for 30 min to obtain a smooth thick slurry. The resulting mixture was ground in an agate mortar after drying at 60 °C in an oven for one night. The black powder was annealed in a tube furnace at 200 °C under 95% Ar /5% H_2 flowing for 3 h. Then, the sample was annealed at 700 °C under 95% Ar /5% H_2 flowing for 2 h to form an ordered intermetallic phase.

Physical Characterizations

The crystalline structures of the PtCo/C and $PtCo_xCu_{1-x}$/C catalysts were determined by X-ray diffraction (XRD) on a Shimadzu XD-3A diffractometer (Japan) and the 2θ diffraction ranges from 5° to 90° with the sweep rate of 2° min^{-1}. The microstructure characteristics and particle distribution were characterized by

transmission electron microscopy (TEM) (JEOL JEM-3010HR). The metal contents of the samples were tested using energy dispersive X-ray spectroscopy (EDX) and inductively coupled plasma-atomic emission spectroscopy (ICP-AES) system (Agilent Technologies, USA). The surface and near-surface of the samples were recorded by an X-ray photoelectron spectrometer (SPECS Surface Nano Analysis GmbH).

Electrochemical measurements

The electrochemical tests of the PtCo/C and $PtCo_xCu_{1-x}$/C catalysts were conducted in a three-electrode cell system on a Zennium electrochemical workstation (Zahner IM6e, Germany). Ag/AgCl was used as the reference electrode; a Pt wire was used as the counter electrode. Pt wire counter electrode purchased from Tianjin Aida is used consistently in our experiments. All the reported potentials were converted to the reversible hydrogen electrode (RHE) scale; the glassy carbon rotating disk working electrode is from Pine Instruments with a surface area of 0.196 cm^2; the catalysts ink was prepared by mixing the catalysts homogenously in 69 ml deionized water, 30 ml isopropyl alcohol, and 1 ml 5wt% Nafion solution to prepare the catalyst inks, 20 µl of the catalyst ink was coated on the GC-RDE surface to prepare a thin layer of the catalysts with loading of 20.4 $\mu g/cm^2_{Pt}$. The cyclic voltammetry (CV) measurements were tested in N_2-saturated 0.1 M $HClO_4$ solution by potential cycling between 0.025 and 1.075 V at a scan rate of 50 mV s^{-1}. The linear sweep voltammetry (LSV) profiles were performed on rotation rate of 1600 rpm in O_2-saturated 0.1 M $HClO_4$ solutions and a scan rate of 10 mV s^{-1} from 0.15 to 1.06 V.

Results and discussion

The XRD profiles of PtCo/C and $PtCo_xCu_{1-x}$/C nanoparticles are shown in **Fig. 1**. The metallic ratio of Cu and Co in the ternary alloy has been adjusted in order to tune the electronic and the crystal phase structure of Pt. The peak position at 2θ of 25° indexes to carbon (200) support material. Compared with monometallic JM Pt/C, the (101) diffraction peak of the PtCo/C catalysts shift toward higher degree. The shift of peak position is a result of the incorporation of Co atoms into Pt lattice to form alloy structure and lead to lattice contraction.[9,38–40] The XRD patterns of the $PtCo_xCu_{1-x}$/C catalysts show similar features as those of PtCo/C. We can see that the (101) peak of $PtCo_xCu_{1-x}$/C appear between those of PtCo/C and JM Pt/C. The (101) peaks shifts slightly to lower angles when the Cu element was introduced, and it shifted even lower with increasing Cu content, the major peak of $PtCo_{0.25}Cu_{0.75}$/C is 0.3° lower then it of $PtCo_{0.75}Cu_{0.25}$/C. This indicates that the increase in lattice parameter caused by the smaller atomic radius Co rather than of Cu.[15] From the XRD results of the PtCo/C and $PtCo_xCu_{1-x}$/C catalysts, the XRD profiles of PtCo/C, $PtCo_{0.75}Cu_{0.25}$/C and $PtCo_{0.5}Cu_{0.5}$/C demonstrates the chemically ordered structure, four additional sharp diffraction peaks appear at about 23° for (001), 33° for (100), 53° for (111), and 58° for (102).[9] These chemically ordered reflections are corresponding to the superlattice peaks of PtCo nanoparticles phase. The formation of superlattice reflections proves the appearance of ordered phase. However, as it can be noticed there is a shoulder appears at the left side off the major peak of $PtCo_{0.5}Cu_{0.5}$/C, which proves that the obtained $PtCo_{0.5}Cu_{0.5}$/C catalyst is a mixture ordered phase (majority) and disordered

phase (minority). The XRD pattern of $PtCo_{0.25}Cu_{0.75}/C$ demonstrated the disappearance of the chemically ordered structure, suggesting over loading of the third transition element Cu will destroy the ordered phase. The particle sizes of the obtained catalysts were calculated from the peak width by using the Scherrer equation.[41] The particle sizes of obtained PtCo/C, $PtCo_{0.75}Cu_{0.25}/C$, $PtCo_{0.5}Cu_{0.5}/C$ and $PtCo_{0.25}Cu_{0.75}/C$ catalysts are 5.1, 5.2, 5.0, and 5.2 nm, respectively.

TEM (as shown in **Fig. 2**) is used to study the morphology and particle distribution details of $PtCo_{0.75}Cu_{0.25}/C$ and $PtCo_{0.25}Cu_{0.75}/C$ nanoparticles. As can be seen from the images, the $PtCo_{0.75}Cu_{0.25}/C$ and $PtCo_{0.25}Cu_{0.75}/C$ catalysts are dispersed uniformly on the supports material without obvious agglomeration. The average crystallite size of catalysts is 5.15 nm and 5.13 nm, respectively. The PtCo/C and $PtCo_{0.5}Cu_{0.5}/C$ catalysts appear similar structural characteristic as shown in **Fig.S1** and **S2**.

The high resolution transmission electron microscopy (HRTEM) images of $PtCo_{0.75}Cu_{0.25}/C$ and $PtCo_{0.25}Cu_{0.75}/C$ catalysts are shown in **Fig. 3**. The HRTEM images reveal that most of the catalysts NPs are spherical with high crystallinity and with well-defined crystal lattice fringes. The crystal lattice fringes prove that the Co, Cu, and Pt atoms were highly alloyed.[36] We confirm the lattice planes can be recognized as the (100) plane of ordered structure $PtCo_{0.75}Cu_{0.25}/C$ phase by evaluating the distance between adjacent atom rows. The formation of the superlattice planes also demonstrates the appearance of chemically ordered structure, which is in agreement with the XRD results. [16,42] However, after the measurement, the lattice

planes can be indexed as the (101) plane of ordered $PtCo_{0.25}Cu_{0.75}$/C phase, indicating the disappearance of the ordered structure. After adding Cu element, the $PtCo_xCu_{1-x}$/C catalysts demonstrated similar microstructure features to those of PtCo/C as observed from the HRTEM and TEM images.

The compositions and surface electronic properties of the PtCo/C and $PtCo_xCu_{1-x}$/C catalysts were measured by EDX, ICP, and XPS analysis. The EDX and ICP results were showed in **Table 1**. The atomic ratios determined were similar to the nominal composition clearly from EDX and ICP analysis. To prove the change of Pt electronic structure, the Pt 4f XPS spectra of PtCo/C and $PtCo_xCu_{1-x}$/C are shown in **Fig. 4**. As observed from the spectra, negative shifts of the Pt 4f binding energy peaks in the $PtCo_xCu_{1-x}$/C catalysts can be seen in contrast to those of PtCo/C catalysts, proving that the electronic property of PtCo is tuned by Cu atoms[41]. In addition, the $PtCo_{0.75}Cu_{0.25}$/C shows a further negative shift in binding energy in than $PtCo_{0.5}Cu_{0.5}$/C, and $PtCo_{0.25}Cu_{0.75}$/C catalysts. These negative shifts in the binding energy demonstrated the change of electronic property, which can reduce the surface oxygen-containing intermediate of $PtCo_xCu_{1-x}$/C catalysts NPs. We also observed two pairs of peaks located at 72.41, 75.36 eV and 71.8, 74.8 eV, which are related to the Pt_{II} and Pt_0, respectively.[43,44] The XPS analysis shows that the Pt is partially oxidized on the surface, which is beneficial for ORR.[45]

Electrochemical Tests

The catalytic performances of the obtained catalysts were measured using RDE in 0.1 M $HClO_4$ solution. For comparison, the JM Pt/C catalysts were measured under

the same condition. All the CV curves of PtCo/C, $PtCo_xCu_{1-x}$/C, and JM Pt/C were given in **Fig. 5(a)**. All the obtained catalysts demonstrate Pt features. The hydrogen desorption/adsorption peaks between 0.05V vs. RHE and 0.4V vs. RHE of $PtCo_xCu_{1-x}$/C shifted to higher potential compared to those of PtCo/C and JM Pt/C, indicating $PtCo_xCu_{1-x}$/C have higher hydrogen binding energy (HBE). The stronger HBE of $PtCo_xCu_{1-x}$/C is attributed to the geometric effect and electronic structure from introducing Cu and Co into the Pt electronic structure.[40,44] In the metal oxidation/reduction region between 0.65V vs. RHE and 0.85V vs. RHE , the $PtCo_{0.75}Cu_{0.25}$/C catalyst shows shift to a higher potential in the backward sweep, implying that the adsorption of affinity of oxygen-containing intermediates on the surface of $PtCo_{0.75}Cu_{0.25}$/C catalysts was much weaker than that on other catalysts. To investigate the Pt utilization, the electrochemically active surface area (ESCA) was calculated by integrating the hydrogen adsorption peak in the potential range 0.05V-0.40V after subtracting the double-layer capacitance and 2.1 C/m^2 for the charge density.[46,47] The results of electrochemical performance test results are listed in **Table 2**.

Fig. 5(b) shows the linear sweep voltammetry (LSV) for ORR activity measurement. For comparison, the curves for the JM Pt/C catalyst are also included. The half-wave potential of the $PtCo_xCu_{1-x}$/C and PtCo/C catalysts is higher than that of JM Pt/C catalyst with an order of JM Pt/C < $PtCo_{0.25}Cu_{0.75}$/C < PtCo/C < $PtCo_{0.5}Cu_{0.5}$/C < $PtCo_{0.75}Cu_{0.25}$/C, indicating rational introduction of the third transition metal can noticeably increase the catalytic activities on the basis of

chemically ordered structure and $PtCo_{0.75}Cu_{0.25}$/C has the optimized ratio of Cu and Co. The half-wave potentials of PtCo/C are much higher than $PtCo_{0.25}Cu_{0.75}$/C, indicating the chemically ordered structure is also important to improve catalytic performance. In order to further study the special structure and atom ratio effect to the catalysts, the specific and mass activities of PtCo/C, $PtCo_{0.75}Cu_{0.25}$/C, $PtCo_{0.5}Cu_{0.5}$/C and $PtCo_{0.25}Cu_{0.75}$/C catalysts at 0.90 V was calculated by the Koutecky–Levich equation. [48] We normalize with ESCA and Pt loading, respectively and list in **table 2**. To calculate the number of electrons transfer of the $PtCo_{0.75}Cu_{0.25}$/C, LSV curves of the at the different rotation rates ranging from 400 to 2500 rpm were used; the LSV curves and corresponding Koutecky–Levich plots were shown in **Fig. S3**. The electrons transferred for the $PtCo_{0.75}Cu_{0.25}$/C catalyst was calculated to be 3.86 between 0.30 and 0.70 V, implying reaction mechanism of O_2 on the catalysts surface by a four-electron reaction process. [49–52]

A superior stability of ORR catalysts is a necessary for fuel cells. The durability measurements of the PtCo/C, $PtCo_{0.75}Cu_{0.25}$/C, and JM Pt/C catalysts were carried out by repeating potential sweeps between 0.06 and 1.10 V for 10000 cycles at a scan rate of 500 mV in N_2-saturated 0.1 M $HClO_4$ electrolyte. Observed in **Fig. 6(a)**, the hydrogen region of JM Pt/C catalysts decreased with potential cycles increase, which is showing poor stability, because of the Pt dissolution, sintering and carbon corrosion. However, PtCo/C catalysts show little change in the hydrogen region after the 3000 potential cycles and then gradual decrease in the subsequent durability measurements in **Fig. 6(c)**. However, the $PtCo_{0.75}Cu_{0.25}$ shows little decrease in hydrogen region in

Fig. 6(e), indicating that the catalytic structure was well reserved. The different change in hydrogen adsorption peak area proves that $PtCo_{0.75}Cu_{0.25}$/C possesses superior structural stability without changes on active lattices and facets than PtCo/C and JM Pt/C. This superior ORR stability can be attributed to the introduction of the third transition metal Cu and the atomic ordered structure.

Fig.6 (b)(d)(f) show the ORR LSV curves of the PtCo/C, JM Pt/C, and $PtCo_{0.75}Cu_{0.25}$ catalysts before and after durability measurements. JM Pt/C shows a larger negative shift of half-wave potential 40 mV, and PtCo/C shows 15 mV decrease. The shift of $PtCo_{0.75}Cu_{0.25}$/C is only 7 mV which is much smaller than that of PtCo/C and JM Pt/C, this shows excellent ORR stability of this catalyst. The excellent catalytic durability is the result of the ordered structure phase of $PtCo_{0.75}Cu_{0.25}$/C and PtCo/C NPs. The $PtCo_{0.75}Cu_{0.25}$/C demonstrated superior durability than the PtCo/C, which is the result of the stabilizing effect of Cu. The durability of the corresponding disordered $PtCo_{0.25}Cu_{0.75}$/C catalyst was shown in Fig.S4.

Conclusion

An impregnation reduction process followed by annealing was used to prepare atomically ordered PtCo/C and $PtCo_xCu_{1-x}$/C catalysts with homogeneously dispersed particle size of ~5 nm. Firstly, we synthesized ordered PtCo/C NPs and annealed at 700 ^{o}C. The catalytic performance of chemically ordered PtCo/C catalysts can be

further promoted by replacing Co with Cu, which obviously tuned the Pt-Pt atoms distance and the surface electric properties. Meanwhile, $PtCo_{0.75}Cu_{0.25}$/C exhibited a significant improvement in catalytic performances for oxygen reduction reaction, which was attributed to the optimum electronic structure and geometric. An obvious enhancement in stability compared with the atomically ordered structure PtCo/C and JM Pt/C electrocatalysts, which was attributed to the fact that the introduction of Cu in the ordered structure $PtCo_{0.75}Cu_{0.25}$/C catalysts to retain the ordered phase under acid environment. The $PtCo_{0.75}Cu_{0.25}$/C catalyst showed excellent catalytic performances compared to JM Pt/C and chemically ordered structure PtCo/C catalyst. This study offers a facile and feasible method for enhancing the catalytic performances of chemically ordered catalysts for catalyzing the ORR.

Acknowledge

We gratefully appreciate the National Natural Science Foundation of China（No. U1705253, No. 21776014, and No. 21776012), the National Key Research and Development Program of China (No. 2016YFB0101203), and the Fundamental Research Funds for the Central Universities (XK1802-6), and the Engineering and Physical Sciences Research Council (EPSRC) grant number: EP/S032886/1.

References

1. M. Cao, D. Wu, and R. Cao, *ChemCatChem*, **6**, 26–45 (2014).
2. C. H. Cui and S. H. Yu, *Acc. Chem. Res.*, **46**, 1427–1437 (2013).
3. M. K. Debe, *Nature*, **486**, 43–51 (2012)
4. Y. Gu, Y. Liu, and X. Cao, *Natl. Sci. Rev.*, **4**, 161–163 (2017).
5. M. Shao, Q. Chang, J. P. Dodelet, and R. Chenitz, *Chem. Rev.*, **116**, 3594–3657 (2016).

6. J. Greeley, I.E.L. Stephens, A.S. Bondarenko, T.P. Johansson, H.A. Hansen, T.F. Jaramillo, J. Rossmeisl, I. Chorkendorff, J.K. Nørskov, *Nat. Chem.*, **1**, 552–556 (2009).
7. V.R. Stamenkovic, B.S. Mun, M. Arenz, K.J.J. Mayrhofer, C.A. Lucas, G. Wang, P.N. Ross, N.M. Markovic, *Nat. Mater.*, **6**, 241–247 (2007).
8. H. A. Gasteiger, S. S. Kocha, B. Sompalli, and F. T. Wagner, *Appl. Catal. B Environ.*, **56**, 9–35 (2005).
9. D. Wang, H.L. Xin, R. Hovden, H. Wang, Y. Yu, D.A. Muller, F.J. Disalvo, H.D. Abruña, *Nat. Mater.*, **12**, 81–87 (2013).
10. B. Arumugam, B.A. Kakade, T. Tamaki, M. Arao, H. Imai, T. Yamaguchi, *RSC Adv.*, **4**, 27510–27517 (2014).
11. J. Kim, Y. Lee, and S. H. Sun, *J. Am. Chem. Soc.*, **132**, 4996 (2010).
12. W. Xiao, W. Lei, M. Gong, H. L. Xin, and D. Wang, *ACS Catal.*, **8**, 3237–3256 (2018).
13. Y. Cai, P. Gao, F. Wang, and H. Zhu, *Electrochim. Acta*, **246**, 671–679 (2017).
14. Y. Liu, N. Chen, F. Wang, Y. Cai, and H. Zhu, *New J. Chem.*, **41**, 6585–6592 (2017).
15. Y. Cai, P. Gao, F. Wang, and H. Zhu, *Electrochim. Acta*, **245**, 924–933 (2017).
16. L. Zou, J. Li, T. Yuan, Y. Zhou, X. Li, H. Yang, *Nanoscale*, **6**, 10686–10692 (2014).
17. B. Arumugam, T. Tamaki, and T. Yamaguchi, *ACS Appl. Mater. Interfaces*, **7**, 16311–16321 (2015).
18. Z. Cui, H. Chen, M. Zhao, and F. J. Disalvo, *Nano Lett.*, **16**, 2560–2566 (2016).
19. M. Bele, P. Jovanovič, A. Pavlišič, B. Jozinović, M. Zorko, A. Rečnik, E. Chernyshova, S. Hočevar, N. Hodnik, M. Gaberšček, *Chem. Commun.*, **50**, 13124–13126 (2014).
20. Y. Zhao, J. Liu, C. Liu, F. Wang, and Y. Song, *ACS Catal.*, **6**, 4127–4134 (2016).
21. M. Chen, B. Lou, Z. Ni, and B. Xu, *Electrochim. Acta*, **165**, 105–109 (2015).
22. G. V. Ramesh, R. Kodiyath, T. Tanabe, M. Manikandan, T. Fujita, N. Umezawa, S. Ueda, S. Ishihara, K. Ariga, H. Abe, *ACS Appl. Mater. Interfaces*, **6**, 16124–16130 (2014).
23. G. V. Ramesh, R. Kodiyath, T. Tanabe, M. Manikandan, T. Fujita, F. Matsumoto, S. Ishihara, S. Ueda, Y. Yamashita, K. Ariga, H. Abe, *ChemElectroChem*, **1**, 728–732 (2014).
24. Y. Zhang, M. Janyasupab, C.W. Liu, X. Li, J. Xu, C.C. Liu, *Adv. Funct. Mater.*, **22**, 3570–3575 (2012).
25. Y. Lu, Y. Jiang, and W. Chen, *Nanoscale*, **6**, 3309–3315 (2014).
26. D. Xiang and L. Yin, *J. Mater. Chem.*, **22**, 9584–9593 (2012).
27. W. Zhong, Y. Liu, and D. Zhang, *J. Phys. Chem. C*, **116**, 2994–3000 (2012).
28. S.M. Alia, G. Zhang, D. Kisailus, D. Li, S. Gu, K. Jensen, Y. Yan, *Adv. Funct. Mater.*, **20**, 3742–3746 (2010).
29. H. Wang, J. Liang, L. Zhu, F. Peng, H. Yu, J. Yang, *Fuel Cells*, **10**, 99–105 (2010).
30. L. Chen, D. Ma, Z. Zhang, Y. Guo, D. Ye, B. Huang, *Catal. Letters*, **142**, 975–

983 (2012).
31. S. S. Kim, C. Kim, and H. Lee, *Top. Catal.*, **53**, 686–693 (2010).
32. Z. Cai, Z. Lu, Y. Bi, Y. Li, Y. Kuang, X. Sun, *Chem. Commun.*, **52**, 3903–3906 (2016).
33. W. Zhu, J. Ke, S.B. Wang, J. Ren, H.H. Wang, Z.Y. Zhou, R. Si, Y.W. Zhang, C.H. Yan, *ACS Catal.*, **5**, 1995–2008 (2015).
34. P. Jovanovič, V.S. Šelih, M. Šala, S.B. Hočevar, A. Pavlišič, M. Gatalo, M. Bele, F. Ruiz-Zepeda, M. Čekada, N. Hodnik, M. Gaberšček, *J. Power Sources*, **327**, 675–680 (2016).
35. Y. Xiong, L. Xiao, Y. Yang, F. J. Disalvo, and H. D. Abruña, *Chem. Mater.*, **30**, 1532–1539 (2018).
36. Z. Xia, P. Zhang, G. Feng, D. Xia, and J. Zhang, *Adv. Mater. Interfaces*, **5**, 1–7 (2018).
37. J. Sun, H. Ma, H. Jiang, L. Dang, Q. Lu, F. Gao, *J. Mater. Chem. A*, **3**, 15882–15888 (2015).
38. L. Xiong and A. Manthiram, *J. Mater. Chem.*, **14**, 1454–1460 (2004).
39. S. Koh, M. F. Toney, and P. Strasser, *Electrochim. Acta*, **52**, 2765–2774 (2007).
40. H. Schulenburg, E. Müller, G. Khelashvili, T. Roser, H. Bönnemann, A. Wokaun, G.G. Scherer, *J. Phys. Chem. C*, **113**, 4069–4077 (2009).
41. L. Yi, L. Liu, X. Wang, X. Liu, W. Yi, X. Wang, *J. Power Sources*, **224**, 6–12 (2013).
42. L. Zou, J. Li, T. Yuan, Y. Zhou, X. Li, H. Yang, *Nat. Commun.*, **6**, 1–9 (2015).
43. M. Chi, C. Wang, Y. Lei, G. Wang, D. Li, K.L. More, A. Lupini, L.F. Allard, N.M. Markovic, V.R. Stamenkovic, *Mater. Chem. Phys.*, **124**, 841–844 (2010).
44. H. Wu, D. Wexler, H. Liu, O. Savadogo, J. Ahn, G. Wang, *J. Power Sources*, **268**, 744–751 (2014).
45. J.N. Zheng, L.L. He, C. Chen, A.J. Wang, K.F. Ma, J.J. Feng, *Int. J. Hydrogen Energy*, **38**, 3323–3329 (2013).
46. H. Zhu, M. Luo, S. Zhang, L. Wei, F. Wang, Z. Wang, Y. Wei, K. Han, *J. Mater. Chem.*, **22**, 23659–23667 (2012).
47. M. Luo, L. Wei, F. Wang, K. Han, and H. Zhu, *J. Power Sources*, **270**, 34–41 (2014).
48. S. Y. Huang, P. Ganesan, S. Park, and B. N. Popov, *J. Am. Chem. Soc.*, **131**, 13898–13899 (2009).
49. X. Liu, X. Wu, and K. Scott, *Catal. Sci. Technol.*, **4**, 3891–3898 (2014).
50. L. Chen, H. Guo, T. Fujita, A. Hirata, W. Zhang, A. Inoue, M. Chen, *Adv. Funct. Mater.*, **21**, 4364–4370 (2011)
51. X. Liu, E. H. Yu, and K. Scott, *Appl. Catal. B Environ.*, **162**, 593–601 (2015)
52. X. Liu, J. Xi, B.B. Xu, B. Fang, Y. Wang, M. Bayati, K. Scott, C. Gao, *Small Methods*, **2**, 1800138 (2018).

Scheme

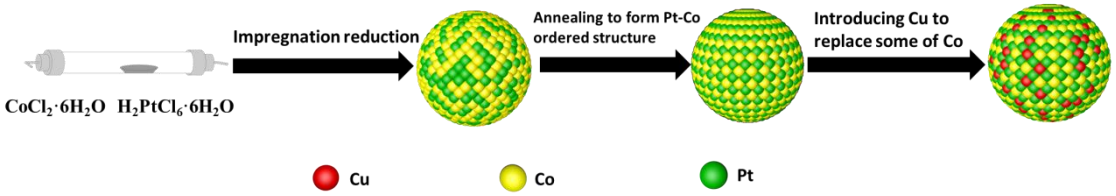

Scheme1 Schematic of synthesis procedure of $PtCo_xCu_{1-x}/C$ catalysts.

Figure Caption

Fig. 1 XRD patterns of PtCo/C, $PtCo_{0.75}Cu_{0.25}/C$, $PtCo_{0.5}Cu_{0.5}/C$ and $PtCo_{0.25}Cu_{0.75}/C$ after annealing at 700 °C for 2 h. The blue, black, and red vertical lines correspond to the peaks of intermetallic PtCu (PDF card # 42-1326), intermetallic PtCo (PDF card # 29-0498), and pure Pt (PDF card # 87-0640), respectively.

Fig. 2 TEM images and particle size histograms of $PtCo_{0.75}Cu_{0.25}/C$ (a, c), and $PtCo_{0.25}Cu_{0.75}/C$ (b, d) catalysts.

Fig. 3 HRTEM images of $PtCo_{0.75}Cu_{0.25}/C$ (a), and $PtCo_{0.25}Cu_{0.75}/C$ (b) catalysts.

Fig. 4 XPS spectra of PtCo, $PtCo_{0.75}Cu_{0.25}/C$, $PtCo_{0.5}Cu_{0.5}/C$, and $PtCo_{0.25}Cu_{0.75}/C$ catalysts in the Pt 4f region.

Fig. 5 (a) CV curves of JM Pt/C, PtCo/C, $PtCo_{0.75}Cu_{0.25}/C$, $PtCo_{0.5}Cu_{0.5}/C$, and $PtCo_{0.25}Cu_{0.75}/C$ catalysts in N_2-saturated 0.1 M $HClO_4$ solution at sweep rate of 50 mV s^{-1}; (b) expanded view of Pt-OH reduction peaks in (a); (c) LSV curves of the catalysts in O_2-saturated 0.1 M $HClO_4$ at rotation rate of 1600 rpm and sweep rate of 10 mV s^{-1}; (d) Mass and specific activities of the catalysts

Fig. 6 CV curves of JM Pt/C (a), PtCo/C (c), and $PtCo_{0.75}Cu_{0.25}/C$ (e) catalysts at different potential cycles in N_2-saturated 0.1 M $HClO_4$ solution at sweep rate of 50 mV s^{-1}; LSV curves of the JM Pt/C (b), Pt_1Co_1/C (c), and $PtCo_{0.75}Cu_{0.25}/C$ (f) catalysts before and after stability test in O_2-saturated 0.1 M $HClO_4$ at rotation rate of 1600 rpm and sweep rate of 10 mV s^{-1}.

Figures

Figure 1

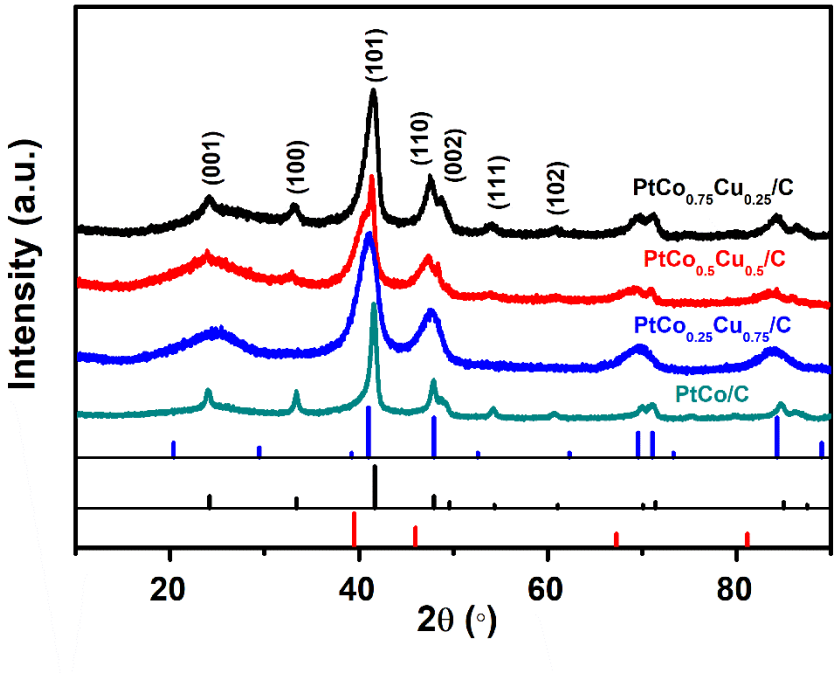

Fig. 1 XRD patterns of PtCo/C, $PtCo_{0.75}Cu_{0.25}$/C, $PtCo_{0.5}Cu_{0.5}$/C and $PtCo_{0.25}Cu_{0.75}$/C after annealing at 700 ºC for 2 h. The blue, black, and red vertical lines correspond to the peaks of intermetallic PtCu (PDF card # 42-1326), intermetallic PtCo (PDF card # 29-0498), and pure Pt (PDF card # 87-0640), respectively.

Figure 2

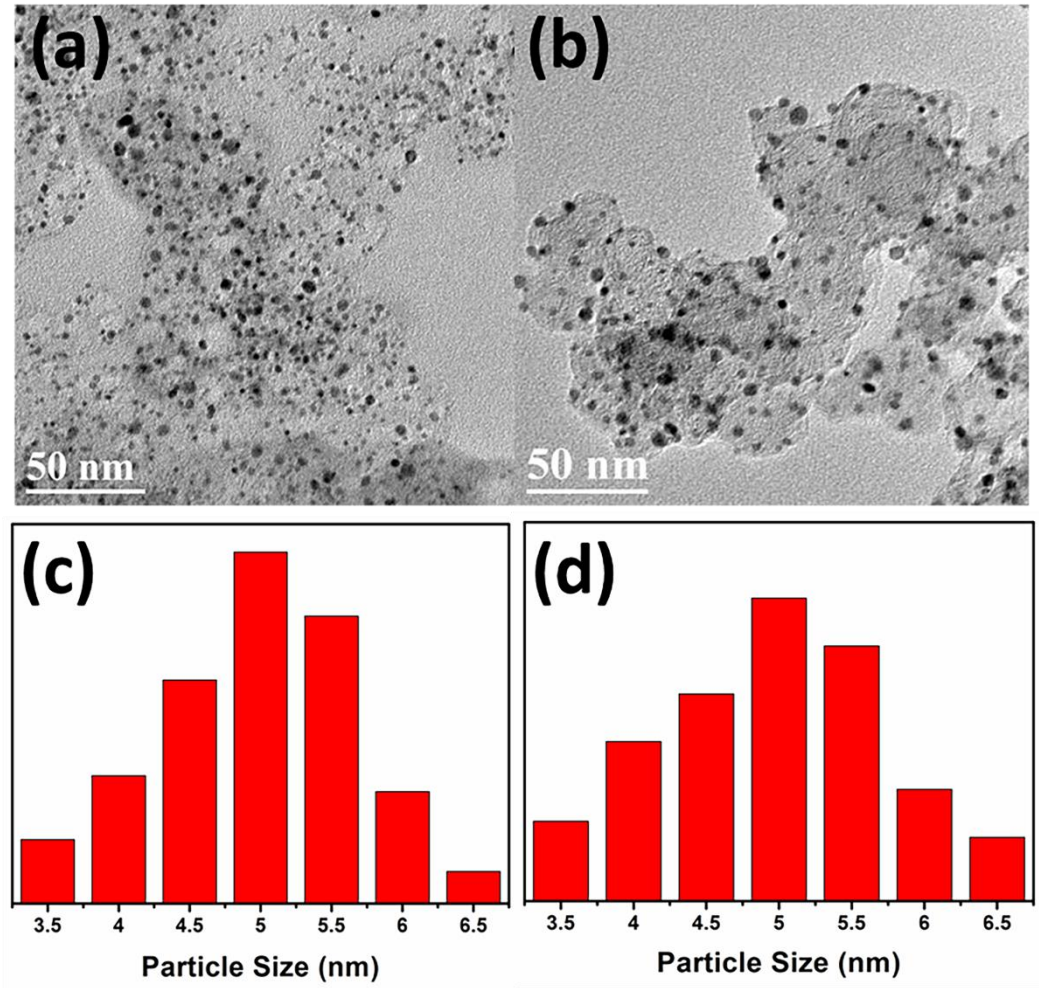

Fig. 2 TEM images and particle size histograms of $PtCo_{0.75}Cu_{0.25}/C$ (a, c), and $PtCo_{0.25}Cu_{0.75}/C$ (b, d) catalysts.

Figure 3

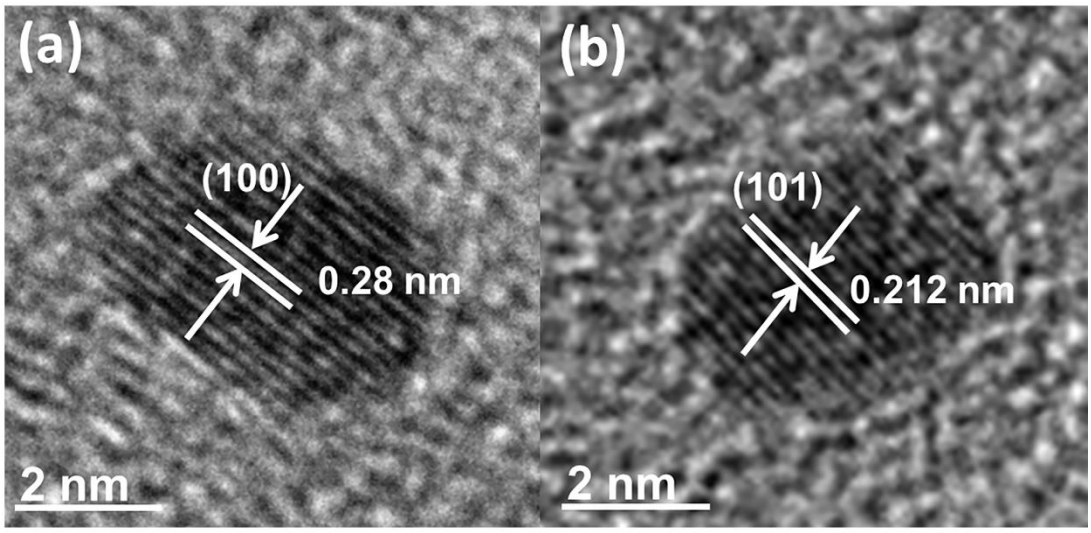

Fig. 3 HRTEM images of $PtCo_{0.75}Cu_{0.25}/C$ (a), and $PtCo_{0.25}Cu_{0.75}/C$ (b) catalysts.

Figure 4

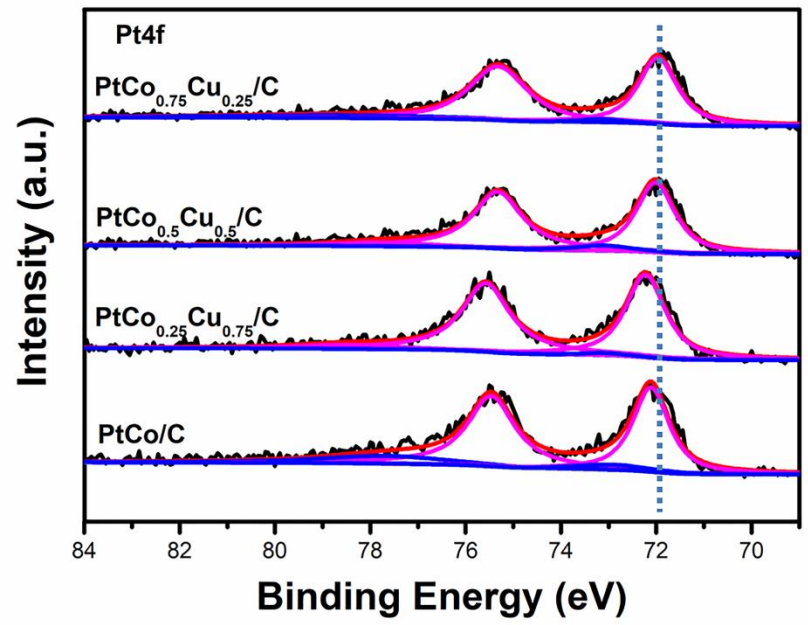

Fig. 4 XPS spectra of PtCo, $PtCo_{0.75}Cu_{0.25}/C$, $PtCo_{0.5}Cu_{0.5}/C$, and $PtCo_{0.25}Cu_{0.75}/C$ catalysts in the Pt 4f region.

Figure 5

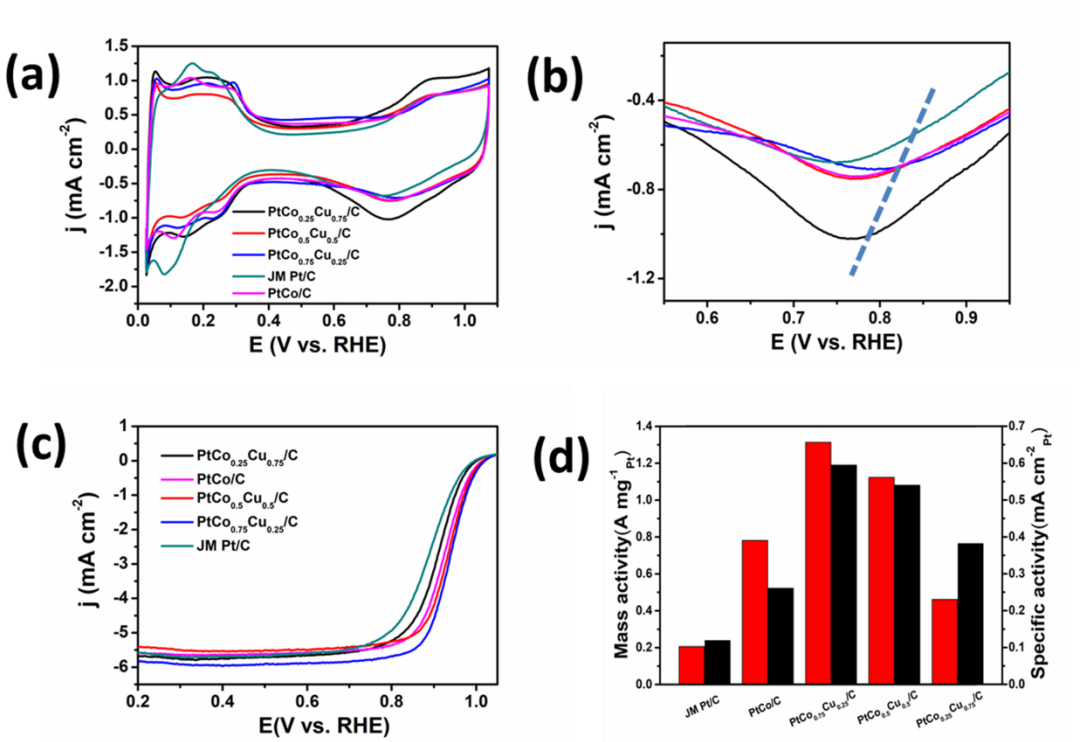

Fig. 5 (a) CV curves of JM Pt/C, PtCo/C, $PtCo_{0.75}Cu_{0.25}$/C, $PtCo_{0.5}Cu_{0.5}$/C, and $PtCo_{0.25}Cu_{0.75}$/C catalysts in N_2-saturated 0.1 M $HClO_4$ solution at sweep rate of 50 mV s^{-1}; (b) expanded view of Pt-OH reduction peaks in (a); (c) LSV curves of the catalysts in O_2-saturated 0.1 M $HClO_4$ at rotation rate of 1600 rpm and sweep rate of 10 mV s^{-1}; (d) Mass and specific activities of the catalysts

Figure 6

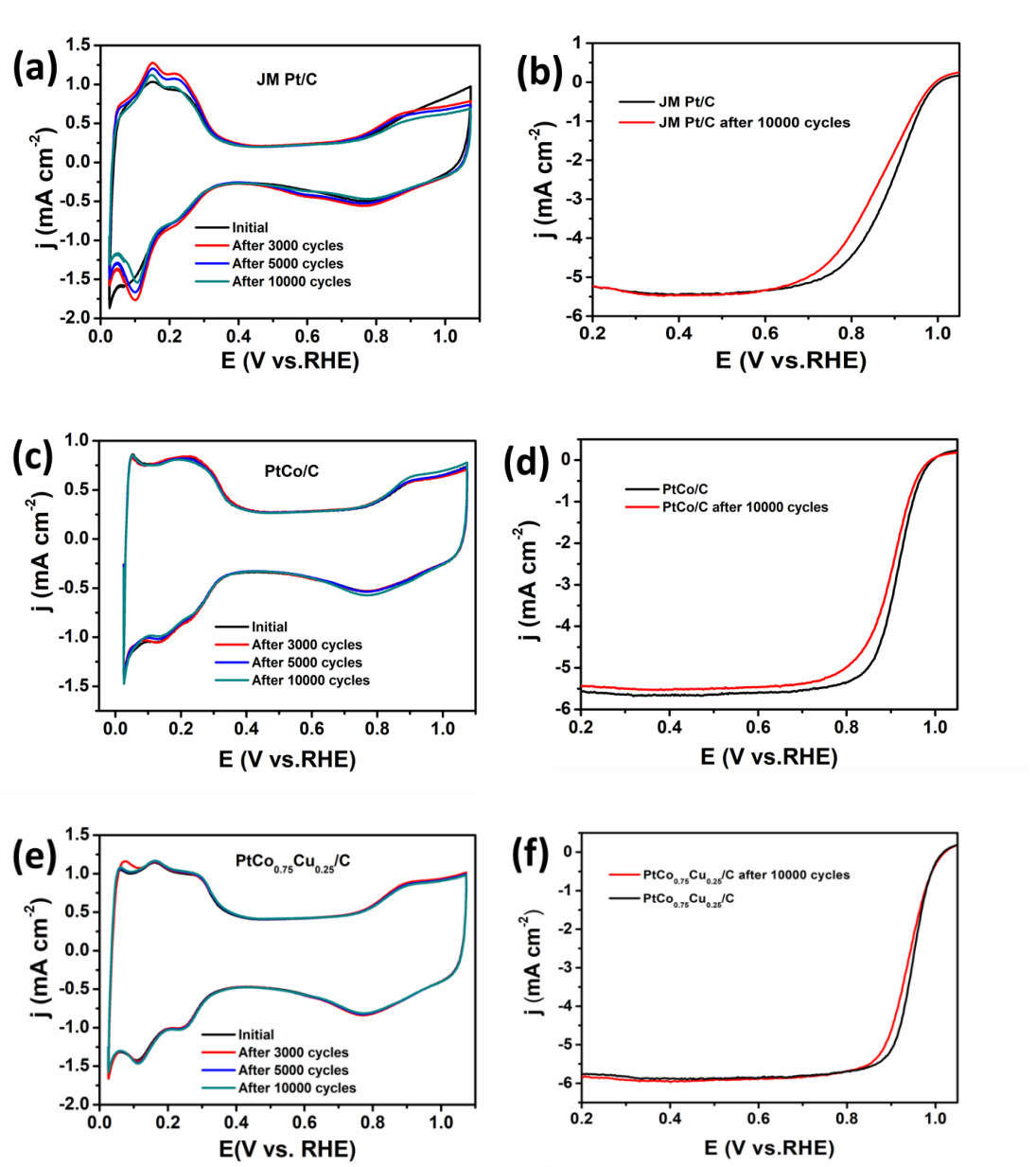

Fig. 6 CV curves of JM Pt/C (a), PtCo/C (c), and $PtCo_{0.75}Cu_{0.25}$/C (e) catalysts at different potential cycles in N_2-saturated 0.1 M $HClO_4$ solution at sweep rate of 50 mV s^{-1}; LSV curves of the JM Pt/C (b), PtCo/C (c), and $PtCo_{0.75}Cu_{0.25}$/C (f) catalysts before and after stability test in O_2-saturated 0.1 M $HClO_4$ at rotation rate of 1600 rpm and sweep rate of 10 mV s^{-1}.

Table(s)

Table 1 Comparison of Pt:Co:Cu atomic ratio determined from EDX and ICP.

Catalysts	**Pt:Co:Cu atomic ratio (EDX)**	**Pt:Co:Cu atomic ratio (ICP)**
PtCo/C	0.97:1	1.01:1
$PtCo_{0.75}Cu_{0.25}/C$	1:0.72:0.27	1:0.73:0.27
$PtCo_{0.5}Cu_{0.5}/C$	1:0.51:0.48	1:0.53:0.49
$PtCo_{0.25}Cu_{0.75}/C$	1:0.28:0.71	1:0.29:0.73

Table 2 Electrochemical performance test results of different catalysts

Catalysts	**ECSA ($m^2g^{-1}_{Pt}$)**	**Mass activity ($A\ mg^{-1}_{Pt}$)**	**Specific activity ($A\ cm^{-2}_{Pt}$)**
JM Pt	172.67	0.20	0.12
PtCo/C	204.61	0.78	0.26
$PtCo_{0.75}Cu_{0.25}/C$	220.60	1.31	0.59
$PtCo_{0.5}Cu_{0.5}/C$	207.92	1.12	0.54
$PtCo_{0.25}Cu_{0.75}/C$	176.67	0.46	0.38